Steel and Composite Structures, *Vol. 21, No. 4 (2016) 755-773*
DOI: http://dx.doi.org/10.12989/scs.2016.21.4.755

A high-order analytical method for thick composite tubes

Hamidreza Yazdani Sarvestani* and Mehdi Hojjati

Department of Mechanical and Industrial Engineering, Concordia University, Montreal, H3G 1M8, Canada

(*Received September 15, 2015, Revised May 24, 2016, Accepted June 01, 2016*)

Abstract. In the present paper, a new high-order simple-input analytical method is used to study thick laminated composite straight tubes subjected to combined axial force, torque and bending moment. The most general displacement field of elasticity for an arbitrary laminated composite straight tube is obtained to analytically calculate stresses under combined loadings based on a layerwise method. The accuracy of the proposed method is subsequently verified by comparing the numerical results obtained using the proposed method with finite element method (FEM) and experimental data. The results show good corresponded. The proposed method provides advantages in terms of computational time compared to FEM.

Keywords: stress analysis; thick laminated composite straight tube; high-order displacement-based method; combined loadings

1. Introduction

Composite tube structures are increasingly used in many aerospace industries. The prediction of the state of stress in different layers of laminated composite tubes is of theoretical interest and subsequently practical applications. In aerospace applications, accurate design and analysis are important to ensure safety and proper performance of composite structures. Note that the stress analysis of thick composite cylindrical structures is often a complex task. A few reasons exist for such a complexity. First, the governing equations of composite tubes are complicated. Second, a major source of intricacy is the layer-wise failure of composite materials. In fact, as soon as a layer fails, a delamination happens or a crack propagates in between the plies, material properties degrade and sometimes the governing equations could be different. Moreover, the tube geometry is a lot more complicated than a flat geometry.

Many researchers have performed investigations on composite straight tubes under different types of loadings. Lekhnitskii (1981) developed the solution for composite tubes under bending load by using partial differential equations. Kollár and Springer (1992) conducted a stress analysis on thin to thick composite tubes under hydrothermal and mechanical loads. Jolicoeur and Cardou (1994) developed a general analytical solution in order to find the stresses and displacements fields of a composite tube subjected to bending, tensile and torsion loads. Tubes made of functionally graded materials (FGM) under tension and bending were analysed (Rooney and Ferrari 2001). An

*Corresponding author, Ph.D. Researcher, E-mail: h_yazd@encs.concordia.ca

http://www.techno-press.org/?journal=scs&subpage=6 ISSN: 1229-9367 (Print), 1598-6233 (Online)

analysis on a cylindrically anisotropic elastic body was made when the body was subjected to extension, torsion, bending and thermo-mechanical loads (Tarn 2001). Shadmehri *et al*. (2011) developed theoretical formulations by using a three-dimensional laminate theory to obtain the stiffness of composite tubes. They compared theoretical formulation with experimental results. Zozulya and Zhang (2012) developed a high order shell theory for FG axisymmetric cylindrical shells based on the expansion of the axisymmetric equations of elasticity. A method was presented to analyze arbitrary laminated composite tubes subjected to pure bending. They performed FEM using NASTRAN to compare with theoretical results (Zhang *et al*. 2014). The stress analysis of composite hollow cylindrical structures subjected to different loadings was performed (Sun *et al*. 2014). Their method was efficient for thin composite hollow tubes. Based on the nonlinear ring theory, mechanical behavior of thermoplastic tubes under combined bending and tension was investigated (Bai *et al*. 2014). They verified formulations with FEM results obtained using ABAQUS. Menshykova and Guz (2014) performed a stress analysis on thick laminated composite tubes subjected to bending loading. They found stresses as a function of the material properties, thickness, lay-up sequences and the magnitude of bending load. Capela *et al*. (2015) investigated the fatigue behavior of composite tubes under bending/torsion dynamic loadings. Recently, a static analysis of a carbon nanotube-reinforced composite tube under thermo-mechanical was studied using Mori-Tanaka theory (Arani *et al*. 2015). A method to obtain and analyze stress distributions in composite cantilever straight tubes was developed (Yazdani Sarvestani 2015, Yazdani Sarvestani *et al*. 2016a, b). The effect of cumulative damage on the seismic behavior of steel tube-reinforced concrete columns through experimental testing was investigated (Ji *et al*. 2014). Nowak and Schmidt (2015) compared some methods to study fiber metal laminated tubes under an axisymmetric load. The developed theoretical model was validated by FEM analyses. Jonnalagadda *et al*. (2015) presented an analytical model for a special design of a thin composites tube subjected to combined bending and torsion. They verified the theoretical results with FEM analyses.

Although many works described above show promise to analyze composite tubes,it is desired to have a method where the inputs(*i.e*., dimensions and lay-up sequences) for the solution are simple; i.e. one only needs to enter the actual dimensions without meshing work. The present work is devoted to develop a high-order analytical method that can provide stresses, strains and deformations with low computational cost for thick laminated composite straight tubes subjected to different mechanical loading conditions such as axial force, torque and bending moment.

2. Motivation

In an effort to develop thermoplastic composite tubes for helicopter landing gears, Derisi (2008) designed and manufactured composite straight tubes and performed four-point and three-point bending tests to determine the strains to failure of different balanced laminates. Derisi used a procedure called strain-controlled design and based on that, lay-up sequences for composite tubes were developed. Even though they have done experimental works, the analytical method does not exist to analyze thick composite straight tubes. Due to the complexity of stress distributions in a thick composite tube, it is not easy to obtain some intuition as to the behavior of the tube under combined loadings, for the purpose of design. Now, in order to provide some insight into this behavior, a new high-order method is developed.

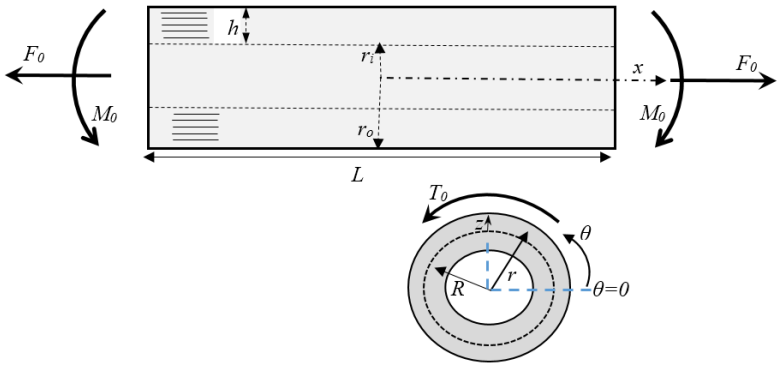

Fig. 1 The geometry of a composite straight tube and the coordinate system

3. Theoretical formulation

3.1 Displacement field

A thick laminated composite straight tube with mean radius R and thickness h is subjected to an axial force F_0, torque T_0 and bending moment M_0 as shown in Fig. 1. The cylindrical coordinates (x, θ, r) are placed at the middle surface of the composite straight tube where x and r are the axial and radial coordinate, respectively. The integration of the appropriate linear strain-displacement relations of elasticity, within cylindrical coordinate system yields the following displacement field for the kth layer (Yazdani Sarvestani *et al*. 2016a)

$$u_1^{(k)}(x,\theta,r) = xr\left(C_5^{(k)}\cos\theta + C_4^{(k)}\sin\theta\right) + C_6^{(k)}x + u^{(k)}(\theta,r) \tag{1a}$$

$$u_2^{(k)}(x,\theta,r) = x\left(C_1^{(k)}\cos\theta - C_2^{(k)}\sin\theta - C_3^{(k)}r\right) - \frac{1}{2}x^2\left(C_4^{(k)}\cos\theta - C_5^{(k)}\sin\theta\right) + v^{(k)}(\theta,r) \tag{1b}$$

$$u_3^{(k)}(x,\theta,r) = x\left(C_1^{(k)}\sin\theta + C_2^{(k)}\cos\theta\right) - \frac{1}{2}x^2\left(C_5^{(k)}\cos\theta + C_4^{(k)}\sin\theta\right) + w^{(k)}(\theta,r) \tag{1c}$$

where $u_1^{(k)}(x,\theta,r)$, $u_2^{(k)}(x,\theta,r)$ and $u_3^{(k)}(x,\theta,r)$ represent the displacementd components in the x, θ and r directions, respectively, of a material point located at (x, θ, r) in the kth ply of the laminated composite straight tube in Fig. 1. In order to satisfy the interfacial continuities of the displacement components, it is necessary that the integration constants appearing in Eqs. (1) to be the same for all layers. Thus, Eqs. (1) are represented as

$$u_1^{(k)}(x,\theta,r) = xr\left(C_5\cos\theta + C_4\sin\theta\right) + C_6x + u^{(k)}(\theta,r) \tag{2a}$$

$$u_2^{(k)}(x,\theta,r) = x\left(C_1\cos\theta - C_2\sin\theta - C_3r\right) - \frac{1}{2}x^2\left(C_4\cos\theta - C_5\sin\theta\right) + v^{(k)}(\theta,r) \tag{2b}$$

$$u_3^{(k)}(x,\theta,r) = x\left(C_1\sin\theta + C_2\cos\theta\right) - \frac{1}{2}x^2\left(C_5\cos\theta + C_4\sin\theta\right) + w^{(k)}(\theta,r) \tag{2c}$$

Moreover, in Eq. (2a), $u^{(k)}(\theta, r)$ can be replaced by $-C_1\sin\theta + u^{(k)}(\theta, r)$. It can be shown that the terms involving C_1 in Eq. (2) correspond to an infinitesimal rigid-body rotation. These terms will, therefore, be ignored in the following developments since they will not generate any strain. Similarly, it can be readily shown that the terms involving C_2 must also be eliminated since they represent another rigid-body rotation of the tube. Furthermore, as long as the loading conditions at both ends of the tube are identical, the constant C_4 must vanish in order to satisfy the symmetry condition in deformation $u_3^{(k)}(x,\theta,r) = u_3^{(k)}(-x,-\theta,r)$. It is thus concluded that the most general form of the displacement field for the *k*th layer of a thick composite straight tube is given as

$$u_1^{(k)}(x,\theta,r) = C_5 xr\cos\theta + C_6 x + u^{(k)}(\theta,r) \tag{3a}$$

$$u_2^{(k)}(x,\theta,r) = -C_3 rx + \frac{1}{2}C_5 x^2\sin\theta + v^{(k)}(\theta,r) \tag{3b}$$

$$u_3^{(k)}(x,\theta,r) = -\frac{1}{2}C_5 x^2\cos\theta + w^{(k)}(\theta,r) \tag{3c}$$

2.2 Layerwise Theory (*LWT*)

The equivalent single-layer theories are not capable of representing the local phenomena in laminated composites, like stress and strain distributions. But then, LWTs, which considerreal *3D* behavior of each layer, are able to present accurate results considering the localized phenomena. In LWT, the displacement components of a generic point in the laminate are conveniently given as (Yazdani Sarvestani and Yazdani Sarvestani 2012)

$$u_1(x,\theta,z) = u_k(x,\theta)\Phi_k(z) \tag{4a}$$

$$u_2(x,\theta,z) = v_k(x,\theta)\Phi_k(z) \tag{4b}$$

$$u_3(x,\theta,z) = w_k(x,\theta)\Phi_k(z) \qquad (k = 1,2,...,N+1) \tag{4c}$$

where *k*, here and in what follows, being a dummy index implying summation of terms from $k = 1$ to $k = N + 1$. In Eqs. (4), u_1, u_2 and u_3 denote the displacement components in the x, θ and z directions, respectively (see Fig. 1). Also, $u_k(x, \theta)$, $v_k(x, \theta)$ and $w_k(x, \theta)$ represent the displacements of the points initially located on the *k*th surface of the laminated composite tube in the x, θ and z directions, respectively. Furthermore, $\Phi_k(z)$ is the global Lagrangian interpolation function that is used for the discretization of the displacement through-thickness and can have linear, quadratic or higher-order polynomial variations of the thickness coordinate z (see *Appendix A*). It is noted that the accuracy of LWT can be enhanced by subdividing each physical layer into a finite number of numerical layers. Clearly, as the number of subdivision through-thickness (p) is increased, the number of governing equations and the accuracy of the results are increased. Based on the elasticity displacement field in Eqs. (3), LWT displacement field in Eqs. (4) is rewritten as

$$u_1(x,\theta,z) = C_5 x(R+z)\cos\theta + C_6 x + U_k(\theta)\Phi_k(z) \tag{5a}$$

$$u_2(x,\theta,z) = -C_3(R+z)x + \frac{1}{2}C_5 x^2\sin\theta + V_k(\theta)\Phi_k(z) \tag{5b}$$

$$u_3(x,\theta,z) = -\frac{1}{2}C_5 x^2 \cos\theta + W_k(\theta)\Phi_k(z)\,(k = 1,2,...,N+1) \tag{5c}$$

It is pointed out here that, by employing through-thickness linear interpolation functions, the continuity of displacement components through the thickness of the laminate is identically satisfied. On the other hand, the transverse strain components remain discontinuous at the interfaces which will subsequently amplify the possibility of having continuous interlaminar stresses at the interfaces of adjacent layers by increasing the number of numerical layers through the physical laminate. By introducing $r = R + z$ (see Fig. 1), the strain-displacement relations are as given as

$$\begin{aligned} &\varepsilon_{xx} = \frac{\partial u_1}{\partial x}, \qquad \varepsilon_{\theta\theta} = \frac{1}{R+z}\frac{\partial u_2}{\partial \theta} + \frac{u_3}{R+z}, \qquad \gamma_{x\theta} = \frac{\partial u_2}{\partial x} + \frac{1}{R+z}\frac{\partial u_1}{\partial \theta} \\ &\gamma_{\theta z} = \frac{1}{R+z}\frac{\partial u_3}{\partial \theta} + \frac{\partial u_2}{\partial z} - \frac{u_2}{R+z}, \qquad \gamma_{xz} = \frac{\partial u_3}{\partial x} + \frac{\partial u_1}{\partial z}, \qquad \varepsilon_{zz} = \frac{\partial u_3}{\partial z} \end{aligned} \tag{6}$$

Substitution of Eqs. (5) into the strain–displacement relations (6) yields the following results

$$\begin{aligned} &\varepsilon_{xx} = (R+z)\left(C_5\cos\theta + C_4\sin\theta\right) + C_6, \qquad \varepsilon_{\theta\theta} = \frac{V_k' + W_k}{R+z}\Phi_k, \qquad \varepsilon_{zz} = W_k\Phi_k' \\ &\gamma_{\theta z} = \frac{W_k' - V_k}{R+z}\Phi_k + V_k\Phi_k', \qquad \gamma_{xz} = U_k\Phi_k' + \left(C_1\sin\theta + C_2\cos\theta\right), \\ &\gamma_{x\theta} = \left(C_1\cos\theta - C_2\sin\theta - C_3(R+z)\right) + \frac{U_k'\Phi_k}{R+z} \end{aligned} \tag{7}$$

In Eq. (7) and what follows, a prime indicates an ordinary differentiation with respect to an appropriate variable (i.e., either θ or z). The equilibrium equations of a thick composite straight tube with numerical layers are obtained by employing Eqs. (7) in the principle of minimum total potential energy (Reisman 1980).The results are, in general, $3(N+1)$ local equilibrium equations corresponding to $3(N+1)$ unknown functions U_k, V_k and W_k and three global equilibrium equations associated with three parameters C_3, C_5 and C_6. Employing the fundamental lemma of calculus of variations, the equilibrium equations of thick laminated composite straight tubes under axial force, torque and bending moment are obtained as

$$\delta U_k : Q_x^k - \frac{dM_{x\theta}^k}{d\theta} = 0 \tag{8a}$$

$$\delta V_k : Q_\theta^k - \frac{dM_\theta^k}{d\theta} - R_\theta^k = 0 \tag{8b}$$

$$\delta W_k : M_\theta^k - \frac{dR_\theta^k}{d\theta} + N_z^k = 0 \tag{8c}$$

$$\delta C_3 : \int_{-\pi}^{\pi}\int_{-h/2}^{h/2} \sigma_{x\theta}(R+z)^2\,dz\,d\theta = T_0 \tag{9a}$$

$$\delta C_5 : \int_{-\pi}^{\pi}\int_{-h/2}^{h/2} \sigma_{xx}(R+z)^2\cos\theta\,dz\,d\theta = M_0 \tag{9b}$$

$$\delta C_6 : \int_{-\pi}^{\pi} \int_{-h/2}^{h/2} R\,\sigma_{xx}\,dz\,d\theta = F_0 \tag{9c}$$

where F_0, T_0, and M_0 represent the prescribed values of the axial force, torque and bending moment, respectively, applied at both ends of the composite straight tube. The generalized stress and moment resultants are defined as

$$\left(N_z^k, Q_x^k, Q_\theta^k\right) = \int_{-h/2}^{h/2} \left(\sigma_{zz}, \sigma_{xz}, \sigma_{\theta z}\right)\Phi_k'\,dz \tag{10a}$$

$$\left(M_\theta^k, M_{x\theta}^k, R_\theta^k\right) = \int_{-h/2}^{h/2} \frac{1}{R+z}\left(\sigma_{\theta\theta}, \sigma_{x\theta}, \sigma_{\theta z}\right)\Phi_k\,dz \tag{10b}$$

Note that in Eqs. (8) and (10), the superscript k refers to the kth surface in the laminated composite tube. Also, the following traction-free boundary conditions must be satisfied

$$R_\theta^k = Q_x^k = N_z^k = 0 \qquad \left(at\ z = \pm h/2\right) \tag{11}$$

By substituting Eq. (7) into three-dimensional constitutive law and the subsequent results into Eqs. (10), the stress resultants are given the following relations

$$\begin{aligned}\left(N_z^k, M_\theta^k, M_{x\theta}^k\right) &= \left(B_{36}^{jk}, H_{26}^{kj}, H_{66}^{kj}\right)U_j' + \left(B_{23}^{jk}, H_{22}^{kj}, H_{26}^{kj}\right)V_j' \\ &+ \left(B_{23}^{jk} + A_{33}^{kj}, H_{22}^{kj} + B_{23}^{kj}, H_{26}^{kj} + B_{36}^{kj}\right)W_j \\ &- \left(\bar{B}_{36}^k, B_{26}^k, B_{66}^k\right)C_3 + \left(\bar{B}_{13}^k, B_{12}^k, B_{16}^k\right)C_5\cos\theta \\ &+ \left(A_{13}^k, F_{12}^k, F_{16}^k\right)C_6\end{aligned} \tag{12}$$

$$\begin{aligned}\left(Q_x^k, Q_\theta^k, R_\theta^k\right) &= \left(A_{55}^{kj}, A_{45}^{kj}, B_{45}^{kj}\right)U_j + \left(B_{45}^{jk}, B_{44}^{jk}, H_{44}^{kj}\right)W_j' \\ &+ \left(A_{45}^{kj} - B_{45}^{jk}, A_{44}^{kj} - B_{44}^{jk}, B_{44}^{kj} - H_{44}^{kj}\right)V_j\end{aligned}$$

where the laminate rigidities in Eq. (12) are defined as

$$\begin{aligned}\left(A_{pq}^{kj}, \bar{B}_{pq}^{kj}, D_{pq}^{kj}\right) &= \sum_{i=1}^{N}\int_{z_i}^{z_{i+1}} \bar{C}_{pq}^{(i)}\left(\phi_k'\phi_j', \phi_k\phi_j', \phi_k\phi_j\right)\mathrm{dz} \\ \left(B_{pq}^{kj}, H_{pq}^{kj}, G_{pq}^{kj}\right) &= \sum_{i=1}^{N}\int_{z_i}^{z_{i+1}} \bar{C}_{pq}^{(i)}\left(\frac{\phi_k\phi_j'}{R+z}, \frac{\phi_k\phi_j}{(R+z)^2}, \frac{\phi_k\phi_j}{R+z}\right)\mathrm{dz} \\ \left(A_{pq}^k, B_{pq}^k, \bar{B}_{pq}^k\right) &= \sum_{i=1}^{N}\int_{z_i}^{z_{i+1}} \bar{C}_{pq}^{(i)}\left(\phi_k', \phi_k, \phi_k'(R+z)\right)\mathrm{dz} \\ \left(D_{pq}^k, F_{pq}^k, E_{pq}^k\right) &= \sum_{i=1}^{N}\int_{z_i}^{z_{i+1}} \bar{C}_{pq}^{(i)}\left(\frac{\phi_k}{(R+z)^2}, \frac{\phi_k}{R+z}, \frac{\phi_k'}{R+z}\right)\mathrm{dz} \\ &\left(k, j = 1, 2, \ldots, N+1\right)\end{aligned} \tag{13}$$

The local displacement equilibrium equations within the proposed method are obtained by substituting Eq. (12) into Eq. (8)

$$\begin{aligned}
\delta U_k :& -H_{66}^{kj}U_j'' + A_{55}^{kj}U_j - H_{26}^{kj}V_j'' - B_{45}^{jk}V_j - \left(H_{26}^{kj} + B_{36}^{kj} - B_{45}^{jk}\right)W_j' = -B_{16}^{k}C_5\sin\theta \\
\delta V_k :& -H_{26}^{kj}U_j'' + \left(A_{45}^{kj} - B_{45}^{kj}\right)U_j - H_{22}^{kj}V_j'' + \left(A_{44}^{kj} - B_{44}^{kj} - B_{44}^{jk} + H_{44}^{kj}\right)V_j \\
& -\left(H_{22}^{kj} + B_{23}^{kj} - B_{44}^{jk} + H_{44}^{kj}\right)W_j' = -B_{12}^{k}C_5\sin\theta \\
\delta W_k :& \left(-B_{45}^{kj} + H_{26}^{kj} + B_{36}^{jk}\right)U_j' + \left(H_{44}^{kj} - B_{44}^{kj} + H_{22}^{kj} + B_{23}^{jk}\right)V_j' - H_{44}^{kj}W_j'' \\
& +\left(H_{22}^{kj} + B_{23}^{jk} + B_{23}^{kj} + A_{33}^{kj}\right)W_j = \left(\bar{B}_{36}^{k} + B_{26}^{k}\right)C_3 - \left(\bar{B}_{13}^{k} + B_{12}^{k}\right)C_5\cos\theta \\
& -\left(A_{13}^{k} + F_{12}^{k}\right)C_6 \\
& k, j = 1, 2, ..., N+1
\end{aligned} \tag{14}$$

Also, the global equilibrium equations of the composite straight tube are expressed in terms of displacement functions by substituting Eq. (7) into three-dimensional constitutive law and the subsequent results into Eqs. (9). The results are given as

$$\begin{aligned}
\delta C_3 :& \frac{1}{h}\int_{-\pi}^{\pi}\left(\bar{B}_{16}C_6 + \bar{D}_{16}C_5\cos\theta + B_{26}^{k}\left(V_j' + W_j\right) + \bar{B}_{36}^{k}W_j - \bar{D}_{66}C_3 + A_{66}^{k}U_j'\right)d\theta = T_0 \\
\delta C_5 :& \int_{-\pi}^{\pi}\begin{pmatrix}\bar{B}_{11}C_6\cos\theta + \bar{D}_{11}C_5\cos^2\theta + B_{12}^{k}\left(V_j' + W_j\right)\cos\theta \\ +F_{13}^{k}W_j\cos\theta - \bar{D}_{16}C_3\cos\theta + B_{16}^{k}U_j'\cos\theta\end{pmatrix}d\theta = M_0 \\
\delta C_6 :& \int_{-\pi}^{\pi}\left(\bar{A}_{11}C_6 + \bar{B}_{11}C_5\cos\theta + F_{12}^{k}\left(V_j' + W_j\right) + B_{13}^{k}W_j - \bar{B}_{16}C_3 + F_{16}^{k}U_j'\right)d\theta = F_0
\end{aligned} \tag{15}$$

where the extra laminate rigidities appearing in Eqs. (15) are written as

$$\begin{aligned}
\left(\bar{A}_{pq}, \bar{B}_{pq}, \bar{D}_{pq}\right) &= \sum_{i=1}^{N}\int_{z_i}^{z_{i+1}}\bar{C}_{pq}^{(i)}\left(1, R+z, (R+z)^2\right)\mathrm{dz} \\
\left(\bar{F}_{pq}, \bar{E}_{pq}\right) &= \sum_{i=1}^{N}\int_{z_i}^{z_{i+1}}\bar{C}_{pq}^{(i)}\left(\frac{1}{R+z}, \frac{1}{(R+z)^2}\right)\mathrm{dz}
\end{aligned} \tag{16}$$

4. Analytical solution

The system in Eqs. (14) shows $3(N+1)$ coupled ordinary differential equations with constant coefficients which may be displayed in a matrix form as follows

$$[M]\{\eta''\} + [K]\{\eta\} = \{F\}\{C\} \tag{17}$$

where

$$\{\eta\}=\left\{\{U\}^T,\{V\}^T,\{\bar{W}\}^T\right\}^T$$
$$\{U\}=\{U_1,U_2,...,U_{N+1}\}^T \qquad \{C\}=\{C_3,C_5,C_6\}^T$$
$$\{V\}=\{V_1,V_2,...,V_{N+1}\}^T \tag{18a}$$
$$\{\bar{W}\}=\{\bar{W}_1,\bar{W}_2,...,\bar{W}_{N+1}\}^T$$

and

$$\bar{W}_j=\int^{\theta} W_j \,\mathrm{d}\theta \tag{18b}$$

The coefficient matrices [*M*], [*K*] and {*F*} in Eq. (17) are defined in Appendix B. It can readily be confirmed that the general solution of Eq. (17) may be presented as

$$\{\eta\}=[\psi]\left[\sinh(\lambda\theta)\right]\{k\}+[K]^{-1}\{F\}\{C\} \tag{19}$$

and [sinh($\lambda\theta$)] is a 3(N+1)× 3(N+1) diagonal matrix. That is

$$\left[\sinh(\lambda\theta)\right]=diag\left(\sinh(\lambda_1\theta),\sinh(\lambda_2\theta),...,\sinh\left(\lambda_{3(N+1)}\theta\right)\right) \tag{20}$$

Also [ψ] and $\left(\lambda_1^2,\lambda_2^2,...,\lambda_{3(N+1)}^2\right)$ are the model matrix and eigenvalues of (–[M]$^{-1}$[K]), respectively. Vector{k} is an unknown vector representing 3(N+1) integration constants. The constants Cj (j = 3, 5 and 6) must be calculated within the analytical analysis. Therefore, the boundary conditions in Eq. (11) are first imposed to calculate the vector $\{k\}$ in terms of the unknown parameters Cj (j = 3, 5 and 6). These constants are then obtained in terms of the specified axial force F_0 or/and bending moment M_0 or/and torque T_0 by the satisfaction of the global equilibrium conditions in Eqs. (15).

5. Lay-up sequence selection

Composite straight tubes with the [90°$_{20}$/0°$_{20}$] and [90°$_{30}$/±25°$_{45}$/90°$_5$/±30°$_{20}$/90°$_5$/±45°$_{20}$] lay-up sequences were manufactured and four-point and three-point bending tests were performed, respectively, to be used for making composite landing gears for helicopters (Derisi 2008). Table 1 shows two types of lay-up sequences considered here. First, the [90°$_{20}$/0°$_{20}$] composite tube is selected to compare the numerical results obtained using the proposed method with finite element

Table 1 Lay-up sequence number

Laminate number	Lay-up sequence	
1	[90°$_{20}$/0°$_{20}$]	Available experimental data
2	[90°$_{30}$/±25°$_{45}$/90°$_5$/±30°$_{20}$/90°$_5$/±45°$_{20}$]	Study stress distributions

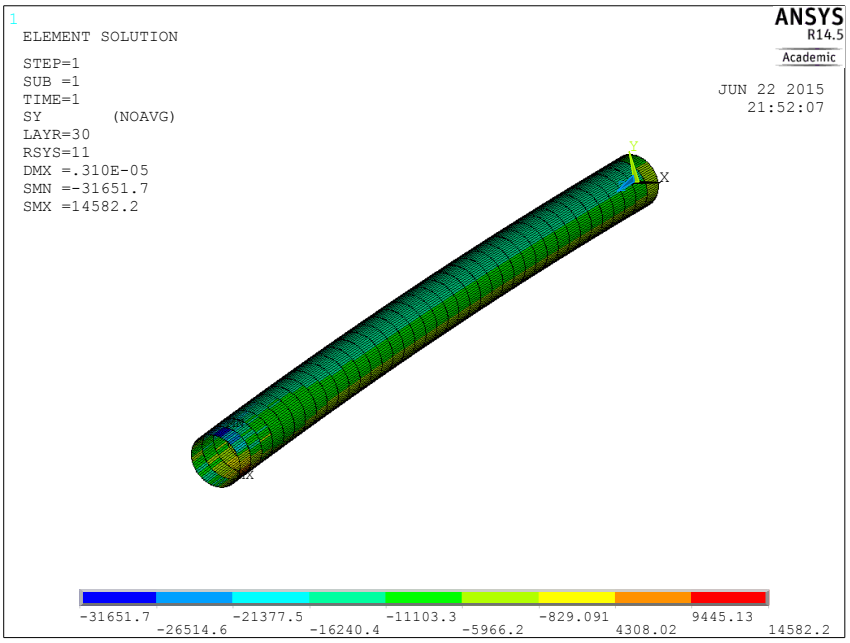

Fig. 2 Distribution of the hoop stress in the composite tube subjected to combined loadings using ANSYS 14.5 (*unit*: *Pa*)

method (ANSYS) and experimental data for the thick laminated composite straight tube subjected to pure bending moment. Finally, the thick $[90°_{30}/\pm25°_{45}/90°_{5}/\pm30°_{20}/90°_{5}/\pm45°_{20}]$ laminated composite tube is considered to study stress distributions in composite straight tubes under combined loading conditions.

6. FEM analysis

The stress analysis of the composite tube is conducted by finite element method using ANSYS. Stress distributions are also generated to compare with the numerical results obtained using the proposed method. The element used to perform the analysis was the layered solid element, SOLID185. The properties of the composite tube are given in Table 2. The composite tubes are modeled according to the manufactured composite tube. The mesh-independency study is done for ANSYS. Mesh refining is performed two times while the element aspect ratio was kept constant. It is emphasized that for the initial mesh, 2268000 elements (90 (*Axial*) × 120 (*circumferential*) × 210 (*thickness directions*)) are used to model the structure. For the 1st refined mesh, the thickness and circumferential directions are refined twice as much as the initial mesh (*9072000 elements totally*). In addition, for the 2nd refined mesh, the axial and circumferential directions are refined twice as much as the initial mesh and the thickness direction is refined 4 times as much as the initial mesh to model the composite tube (*36288000 elements totally*). Fig. 2 presents the hoop stress distribution along the length inthe thick laminated composite straight tube using ANSYS 14.5.

7. Results and discussion

Numerical results are presented in four sections. First, in Section 7.1, the comparison is made between the experimental data with those obtained using the present method. Second, in Section 7.2, the numerical results obtained by the proposed method are compared with FEM results. Third, in Section 7.3, the advantages of the proposed method over FEM and other methods are discussed. Finally, in Section 7.4, stress distributions in thick laminated composite straight tubes subjected to axial force, torque and bending moment are studied. In all the subsequent calculations, p is set equal to 12 (Yazdani Sarvestani *et al*. 2016a). The mechanical properties of the composite tube are given in Table 2 (Derisi 2008).

Furthermore, the stress components are normalized as $\bar{\sigma}_{ij} = \sigma_{ij}/\sigma_0$ where $\sigma_0 = (M_0.r)/(\pi/64*(OD^4\text{-}ID^4)) + (T_0.r)/(\pi/32*(OD^4\text{-}ID^4)) + (F_0)/(\pi/4*(OD^2\text{-}ID^2))$ where the outer diameter and the inner diameter of the composite straight tube are represented as OD and ID, respectively. In the present cases, the tube section with the $[90°_{30}/\pm25°_{45}/90°_5/\pm30°_{20}/90°_5/\pm45°_{20}]$ lay-up sequence has an internal diameter of 56 mm and an external diameter of 98 mm, i.e., a wall thickness of 21 mm (totally 210 layers). Also, the length of the composite straight tube is 405 mm. Thickness is kept constant for all physical layers (Derisi 2008). Note that in this paper, mentioning combined loadings are meant by all loading conditions (i.e., axial force, torque and bending moment) are applied together. In addition, remark that M_0 = 10 N.m, T_0 = 10 N.m and F_0 =10 N are assumed.

7.1 Comparison of the proposed method with experimental data

In this part, the proposed method results are compared with experimental data.The bending behavior of thick composite tubes was investigated experimentally (Derisi 2008). The $[90°_{20}/0°_{20}]$ thick thermoplastic composite tubes were manufactured using automated fiber placement technique and tested using a four-point bending test setup. The properties of the manufactured composite tube are given in Table 2. In the experimental case, the tube section has an internal diameter of 56 mm and an external diameter of 64 mm. Also, the whole length of the composite tube is 810 mm while the tube length under the pure bending condition is 405 mm. The composite tube was made with 40 layers. Since four-point bending test results are available, the composite tube is studied under pure bending moment just to compare with experimental data. In the experimental investigation (Derisi 2008), the strain gage was used on the surface of the composite tube at the top line of the tube (θ = 90°) to measure strains at the mid-span. The measured strain results are compared with the calculated strain results using the proposed method at θ = 90°. In Fig. 3, the force variation versus experimental axial strains is shown. Good agreement is obtained between the analytical analysis and experimental results. In addition, FEM (ANSYS) (see Fig. 3) is used to evaluate the accuracy of the proposed method. It is seen that the proposed method results are closer to the experimental data compared to those of FEM (ANSYS). Also, the results obtained using the proposed method show good correspondence at the higher level of load compared to those of FEM. It is noted that the 2nd refined mesh (see Section 6) is used to get FEM results here.

Table 2 Mechanical properties of the manufactured composite tube

Properties	E_1 (GPa)	$E_2 = E_3$ (GPa)	$G_{12} = G_{13} = G_{23}$ (GPa)	$v_{12} = v_{13}$	v_{23}
Carbon AS4/PEEK	140	10	5.56	0.31	0.33

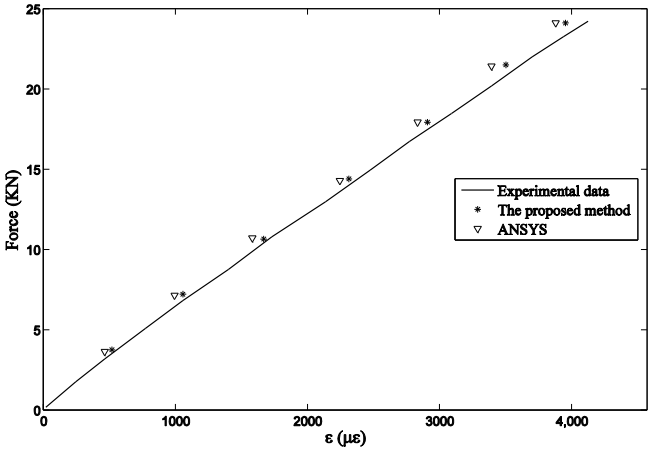

Fig. 3 Force-axial strain at the top line of the tube (θ = 90°)

7.2 Comparison of the proposed method and FEM

The interlaminar stresses, $\bar{\sigma}_{zz}$ and $\bar{\sigma}_{zx}$, of the $[90°_{30}/\pm25°_{45}/90°_{5}/\pm30°_{20}/90°_{5}/\pm45°_{20}]$ laminated composite straight tube under combined loadings at r = 31 mm and r = 40 mm obtained by the present method and FEM (ANSYS) are compared in Fig. 4. Good agreement is observed between analytical analysis and FEM (ANSYS) results. Analyzing of the composite straight tube with the initial mesh takes around 1200 seconds while it takes around 2100 and 4200 seconds with the 1st refined and the 2nd refined meshes, respectively. But the analyzing of the same structure (*same complex lay-up*) using the developed method takes 560 seconds.

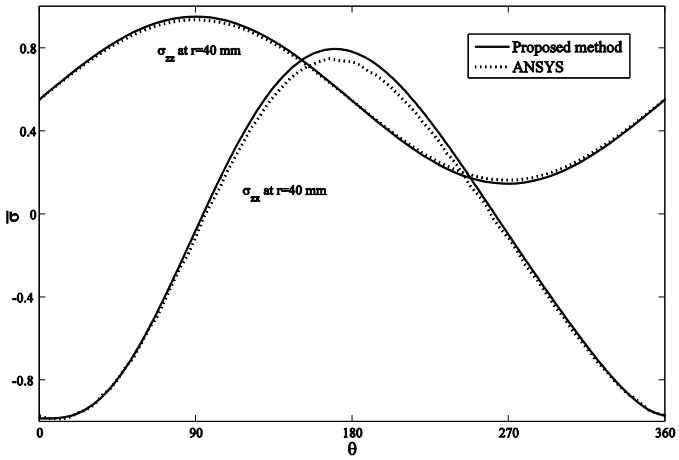

Fig. 4 Comparison of the radial and shear stresses, $\bar{\sigma}_{zz}$ and $\bar{\sigma}_{zx}$, obtained from the proposed method and ANSYS of the $[90°_{30}/\pm25°_{45}/90°_{5}/\pm30°_{20}/90°_{5}/\pm45°_{20}]$ laminated composite straight tube

7.3 Advantages of the proposed method

FEM has a unique limitation: every time the geometry, loading, lay-up sequences or materials change, simulations need to be carried our afresh, which might involve new mesh generation and computation. The most important advantage of the proposed method is that inputs for the modeling of composite structures with complex lay-up sequences (see Table 1) are simple, easy to use, and fast to run. Contrary, to model complex lay-up composite structures in FEM, it is necessary to create individual sections and mesh them separately with different lay-up attributes. But, through using the proposed method, it is required to simply input dimensions and lay-up sequences at the beginning of the program. Therefore, it is obvious that the modeling of composite structures with complex lay-up sequences using FEM takes much longer compared to using the developed method. In addition, the proposed method takes less computational time as compared to the conventional 3D FEM and providing the better level of accuracy. (See Section 7.2)

One of the other advantages of the developed method is the accuracy of the obtained results (see Fig. 3). It was shown that the results obtained using the proposed method is more accurate than FEM results compared to experimental data. In addition, using FEM for parametric study is cumbersome while this method can be applied easily for any parametric study with low computational cost. For example, to study the effects of thickness on stress and strain distributions by using FEM, it is necessary to model the geometry for different thicknesses and obviously it takes much longer than using the present method.

7.4 Stress distributions

The thick $[90°_{30}/\pm25°_{45}/90°_{5}/\pm30°_{20}/90°_{5}/\pm45°_{20}]$ laminated composite tube which has 210 layers in total is selected to study stress distributions of the thick composite straight tube subjected to axial force, torque and bending moment. The results are presented based on the proposed method at r = 31 mm (the last 90°-ply of the first 90° layer-group from inside, i.e., *layer 30*), r =

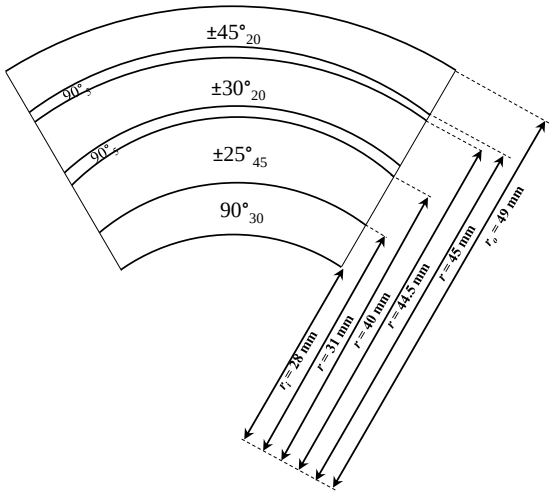

$[90°_{30}/\pm25°_{45}/90°_{5}/\pm30°_{20}/90°_{5}/\pm45°_{20}]$

Fig. 5 The lay-up sequenceof thethick laminatedcompositestraight tube

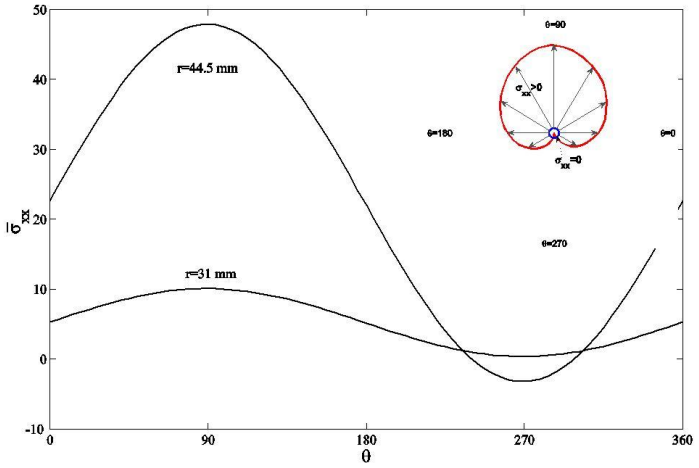

(a)

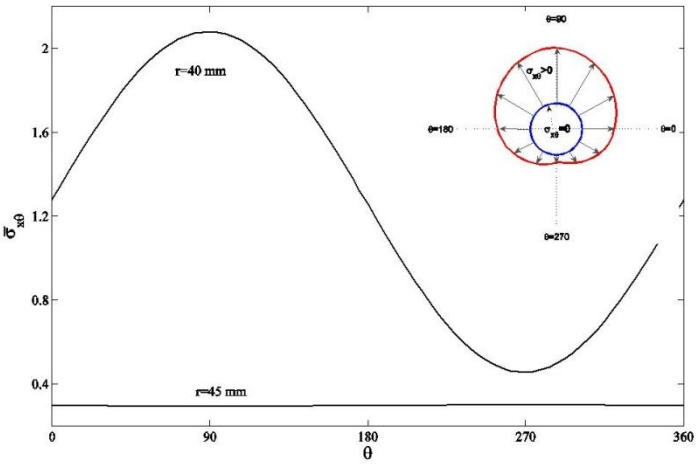

(b)

Fig. 6 (a) Distributions of the axial stress $\bar{\sigma}_{xx}$ of the $[90°_{30}/\pm25°_{45}/90°_{5}/\pm30°_{20}/90°_{5}/\pm45°_{20}]$ laminated composite straight tube; (b) Distributions of the shear stress $\bar{\sigma}_{x\theta}$ of the $[90°_{30}/\pm25°_{45}/90°_{5}/\pm30°_{20}/90°_{5}/\pm45°_{20}]$ laminated composite straight tube

40 mm (the last 25°-ply of the ±25° layer-group, i.e., *layer* 120), r = 44.5 mm (the last 30°-ply of ±30° layer-group, i.e., *layer 165*) and r = 45 mm (the last 90°-ply of the third 90° layer-group, i.e., *layer 170*) as shown in Fig. 5.

The distributions of the axial, $\bar{\sigma}_{xx}$, and shear stresses, $\bar{\sigma}_{x\theta}$, of the thick $[90°_{30}/\pm25°_{45}/90°_{5}/\pm30°_{20}/90°_{5}/\pm45°_{20}]$ laminated composite tube along the circumferential direction are shown in Figs. 6(a) and (b). It is seen that the axial, $\bar{\sigma}_{xx}$, and shear stresses, $\bar{\sigma}_{x\theta}$, have an anti-symmetric behavior. In addition, the shear stress, $\bar{\sigma}_{x\theta}$, is positive at the whole tube cross section while the axial stress, $\bar{\sigma}_{xx}$, is negative at a part of the lower region of the tube cross section (180°-360°). In addition, to understand better the stress behavior, the polar distribution of the axial stress, $\bar{\sigma}_{xx}$, and the shear stress, $\bar{\sigma}_{x\theta}$, at r = 44.5 mm and r = 40 mm of the thick laminated composite tube obtained by the present method is shown in Figs. 6(a) and (b), respectively. Note that in all polar distributions in

the rest of the paper, blue circle represents the zero stress condition while red lines represent the stress distributions. Also, the lengths of arrows represent the magnitudes of stresses. Therefore, those red lines where are placed inside the blue circle represent the compressive stress while the other red lines where are placed outside of the blue circle represent the tensile stress.

The distributions of the interlaminar radial stress, $\bar{\sigma}_{zz}$, and the shear stress,$\bar{\sigma}_{zx}$, of the [90°$_{30}$/±25°$_{45}$/90°$_{5}$/±30°$_{20}$/90°$_{5}$/±45°$_{20}$] laminated composite tube along the circumferential direction are shown in Fig. 7(a). The positive maximum value of the interlaminar normal stress, $\bar{\sigma}_{zz}$, occurs at θ = 270°. It is noted that the positive radial stress, $\bar{\sigma}_{zz}$, can cause delamination phenomena in the cross section of composite tube. The magnitude of the interlaminar radial stress, $\bar{\sigma}_{zz}$, is greater than that of the shear stress $\bar{\sigma}_{zx}$. Fig. 7(b) presents the polar distributions of the interlaminar radial stress, $\bar{\sigma}_{zz}$, and the shear stress, $\bar{\sigma}_{zx}$, of the [90°$_{30}$/±25°$_{45}$/90°$_{5}$/±30°$_{20}$/90°$_{5}$/±45°$_{20}$] laminated

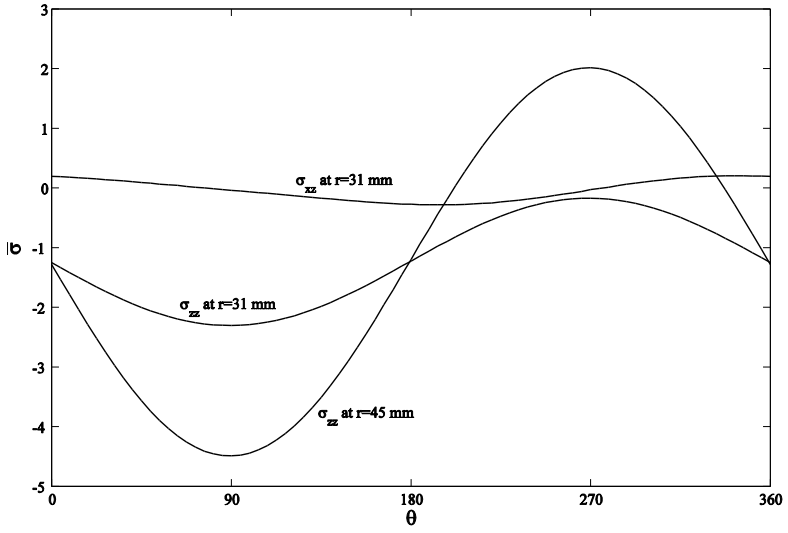

Fig. 7 (a) Distributions of the interlaminar radial stress $\bar{\sigma}_{zz}$ and shear stress $\bar{\sigma}_{zx}$ of the [90°$_{30}$/±25°$_{45}$/90°$_{5}$/±30°$_{20}$/90°$_{5}$/±45°$_{20}$] laminated composite straight tube; (b) Polar distributions of the interlaminar radial stress $\bar{\sigma}_{zz}$ and shear stress $\bar{\sigma}_{zx}$ of the [90°$_{30}$/±25°$_{45}$/90°$_{5}$/±30°$_{20}$/90°$_{5}$/±45°$_{20}$] laminated composite straight tube

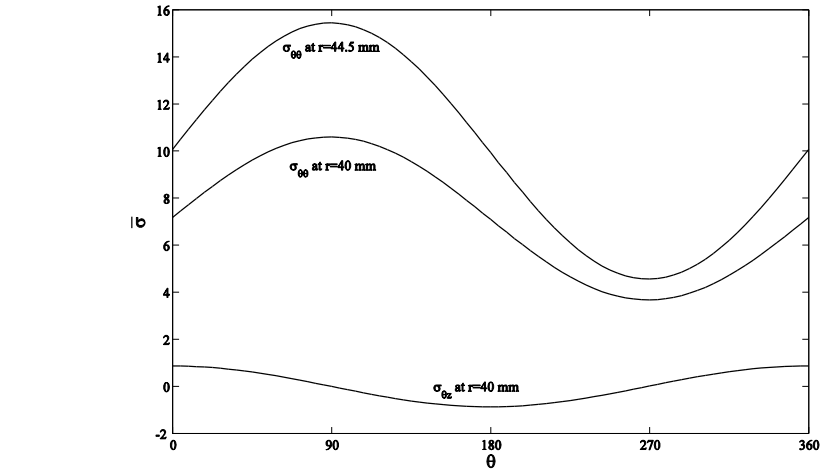

(a)

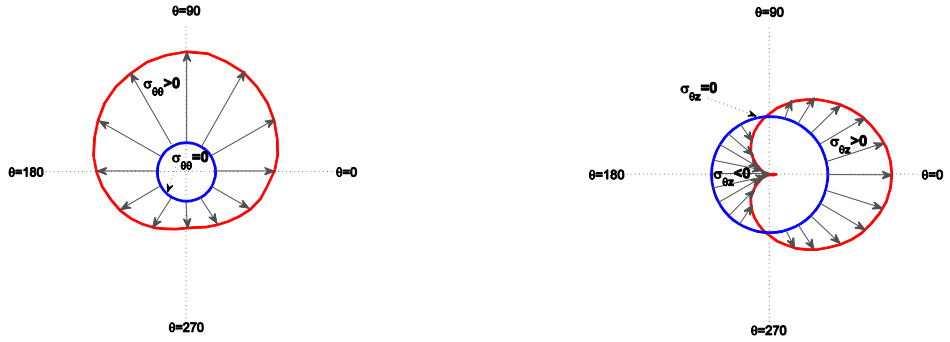

(b)

Fig. 8 (a) Distributions of the hoop stress $\bar{\sigma}_{\theta\theta}$ and shear stress $\bar{\sigma}_{\theta z}$ of the [90°$_{30}$/±25°$_{45}$/90°$_{5}$/±30°$_{20}$/90°$_{5}$/±45°$_{20}$] laminated composite straight tube; (b) Polar distributions of the hoop stress $\bar{\sigma}_{\theta\theta}$ and shear stress $\bar{\sigma}_{\theta z}$ of the [90°$_{30}$/±25°$_{45}$/90°$_{5}$/±30°$_{20}$/90°$_{5}$/±45°$_{20}$] laminated composite straight tube

composite tube over cross section at r = 45 mm and r = 31 mm, respectively, obtained based on the present method.

Fig. 8(a) presents the distributions of the hoop stress, $\bar{\sigma}_{\theta\theta}$, and the shear stress, $\bar{\sigma}_{\theta z}$, of the [90°$_{30}$/±25°$_{45}$/90°$_{5}$/±30°$_{20}$/90°$_{5}$/±45°$_{20}$] laminated composite tube along the circumferential direction. It is observed that the hoop stress, $\bar{\sigma}_{\theta\theta}$, is positive at the upper region of the tube cross section while the shear stress, $\bar{\sigma}_{\theta z}$, sign changes in this region (0°-180°). The maximum value of the hoop stress, $\bar{\sigma}_{\theta\theta}$, occurs at θ = 90° while maximum value of the shear stress, $\bar{\sigma}_{\theta z}$, occurs at θ = 0°. Fig. 8(b) presents the polar distributions of the hoop stress, $\bar{\sigma}_{\theta\theta}$, and the shear stress, $\bar{\sigma}_{\theta z}$, of the [90°$_{30}$/±25°$_{45}$/90°$_{5}$/±30°$_{20}$/90°$_{5}$/±45°$_{20}$] laminated composite tube over cross section at r = 44.5 mm and r = 40 mm, respectively, obtained based on the present method.

Since the radial stress affects delamination and the hoop stress affects buckling, the interlaminar radial and hoop stresses distributions along the tube thickness are studied. The distributions of the interlaminar radial stress,$\bar{\sigma}_{zz}$, and the hoop stress, $\bar{\sigma}_{\theta\theta}$, of the [90°$_{30}$/±25°$_{45}$/90°$_{5}$/±30°$_{20}$/90°$_{5}$/±45°$_{20}$] laminated composite tube under pure bending moment along the

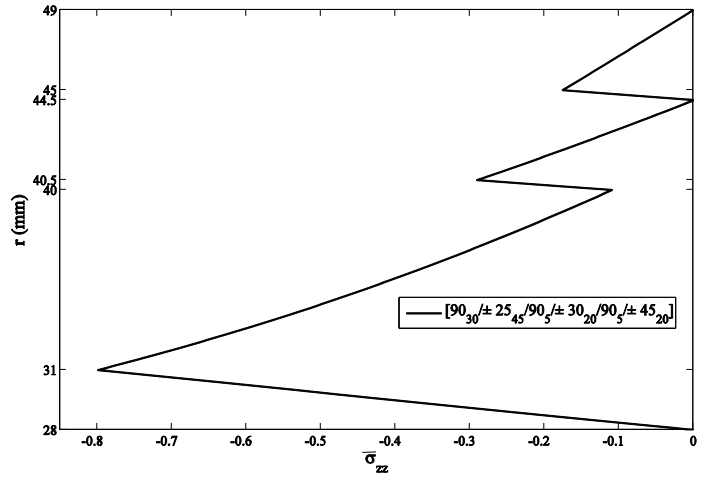

(a)

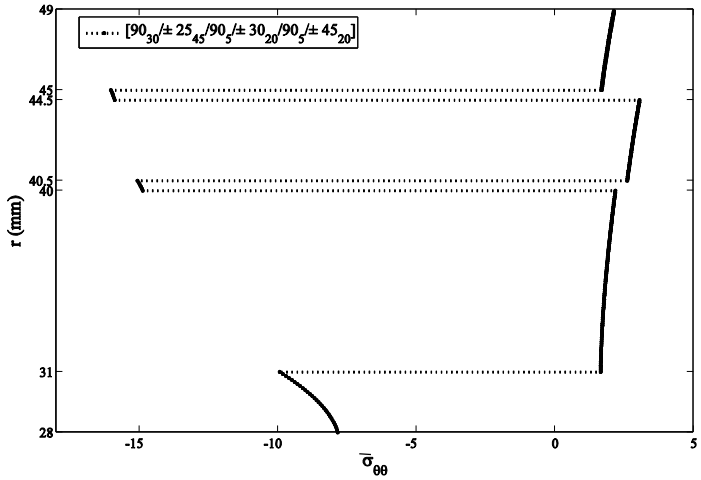

(b)

Fig. 9 (a) Distributions of the interlaminar radial stress $\bar{\sigma}_{zz}$ of the [90°$_{30}$/±25°$_{45}$/90°$_5$/±30°$_{20}$/90°$_5$/±45°$_{20}$] laminated composite straight tube along the thickness at θ = 90°; (b) Distributions of the hoop stress $\bar{\sigma}_{\theta\theta}$ of the [90°$_{30}$/±25°$_{45}$/90°$_5$/±30°$_{20}$/90°$_5$/±45°$_{20}$] laminated composite straight tube along the thickness at θ = 90°

thickness at θ = 90° are shown in Figs. 9(a) and (b), respectively. It is seen that the radial stress, $\bar{\sigma}_{zz}$, is compressive totally along the tube thickness while the hoop stress, $\bar{\sigma}_{\theta\theta}$, is compressiveat the inside surface and becoming positive by closing to the outside surface of the composite straight tube. As it is expected from Eqs. (11), Fig. 9(a) shows that the interlaminar radial stress, $\bar{\sigma}_{zz}$, is zero at the inside and outside surfaces of the laminated composite tube (N_z^k = 0 at $z = \pm h/2$). The maximum value of the radial stress, $\bar{\sigma}_{zz}$, occurs at r = 31 mm along the thickness, where the last 90°-ply of the first 90° layer-group is placed. While the maximum magnitude of the hoop stress, $\bar{\sigma}_{\theta\theta}$, occurs at r = 45 mm, where the last 90°-ply of the third 90° layer-group is placed.

8. Conclusions

A new high-order simple-input displacement-based method was developed to investigate stresses in thick laminated composite straight tubes subjected to axial force, torque and bending moment. LWT was used to analytically determine the displacement components considering the most general displacement field of elasticity. The equilibrium equations of LWT were subsequently derived through a state-space approach. Also, the accuracy of the results was studied by comparing the experimental data and FEM with numerical results obtained from the proposed method. Good agreement was seen. Furthermore, the stresses were obtained using the present method which was shown to be more cost effective and accurate compared to FEM.

Acknowledgments

The financial contributions from the Natural Sciences and Engineering Research Council of Canada (NSERC), Bell Helicopter Textron Canada Ltd. and Concordia University are appreciated.

References

Arani, A.G., Haghparast, E., Maraghi, Z.K. and Amir, S. (2015), "Static stress analysis of carbon nano-tube reinforced composite (CNTRC) cylinder under non-axisymmetric thermo-mechanical loads and uniform electro-magnetic fields", *Compos. Part B: Eng.*, **68**, 136-145.

Bai, Y., Ruan, W., Cheng, P., Yu, B. and Xu, W. (2014), "Buckling of reinforced thermoplastic pipe (RTP) under combined bending and tension", *Ships Offshore Struct.*, **9**(5), 525-539.

Capela, C., Ferreira, J.A.M., Febra, T. and Costa, J.D. (2015), "Fatigue strength of tubular carbon fibre composites under bending/torsion loading", *Int. J. Fatigue*, **70**, 216-222.

Derisi, B. (2008), "Development of thermoplastic composite tubes for large deformation", Ph.D. Dissertation; Concordia University, Montreal, QB, Canada.

Ji, X., Zhang, M., Kang, H., Qian, J. and Hu, H. (2014), "Effect of cumulative seismic damage to steel tube-reinforced concrete composite columns", *Earthq. Struct., Int. J.*, **7**(2), 179-119.

Jolicoeur, C. and Cardou, A. (1994), "Analytical solution for bending of coaxial orthotropic cylinders", *J. Eng. Mech.*, **120**(12), 2556-2574.

Jonnalagadda, A.K., Sawant, A.S., Rohde, S.R., Sankar, B.V. and Ifju, P.G. (2015), "An analytical model for composite tubes with bend-twist coupling",*Compos. Struct.*, **131**, 578-584.

Kollár, L. and Springer, G.S. (1992), "Stress analysis of anisotropic laminated cylinders and cylindrical segments", *Int. J. Solid. Struct.*, **29**(12), 1499-1517.

Lekhnitskii, S.G. (1981), *Theory of Elasticity of an Anisotropic Body*, Mir Publisher, Moscow, Russia.

Menshykova, M. and Guz, I.A. (2014), "Stress analysis of layered thick-walled composite pipes subjected to bending loading", *Int. J. Mech. Sci.*, **88**, 289-299.

Nowak, T. and Schmidt, J. (2015), "Theoretical, numerical and experimental analysis of thick walled fiber metal laminate tube under axisymmetric loads", *Compos. Struct.*, **131**, 637-644.

Reisman, H. (1980), *Elasticity Theory and Applications*, John Wily & Sons, New York, NY, USA.

Rooney, F. and Ferrari, M. (2001), "Tension, bending, and flexure of functionally graded cylinders", *Int. J. Solid. Struct.*, **38**(3), 413-421.

Shadmehri, F., Derisi, B. and Hoa, S.V. (2011), "On bending stiffness of composite tubes", *Compos. Struct.*, **93**(9), 2173-2179.

Sun, X.S., Tan, V.B.C., Chen, Y., Tan, L.B., Jaiman, R.K. and Tay, T.E. (2014), "Stress analysis of multi-layered hollow anisotropic composite cylindrical structures using the homogenization method", *Acta Mechanica*, **225**(6), 1649-1672.

Tarn, J. (2001), "Exact solutions for functionally graded anisotropic cylinders subjected to thermal and mechanical loads", *Int. J. Solid. Struct.*, **38**(46-47), 8189-8206.
Yazdani Sarvestani, H. (2015), "Effects of layup sequences on stresses of thick composite cantilever tubes", *Adv. Compos. Mater.*, **1**, 21.
Yazdani Sarvestani, H. and Yazdani Sarvestani, M. (2011), "Interlaminar stress analysis of general composite laminates", *Int. J. Mech. Sci.*, **53**(11), 958-967.
Yazdani Sarvestani, H. and Yazdani Sarvestani, M. (2012), "Free-edge stress analysis of general composite laminates under extension, torsion and bending", *Appl. Math. Model.*, **36**(4),1570-1588.
Yazdani Sarvestani, H., Hoa, S.V. and Hojjati, M. (2016a), "Stress analysis of thick orthotropic cantilever tubes under transverse loading", *Adv. Compos. Mater.*, 1-28.
Yazdani Sarvestani, H., Hoa, S.V. and Hojjati, M. (2016b), "Effects of shear loading on stress distributions at sections in thick composite tubes", *Compos. Struct.*, **140**, 433-445.
Zhang, C., Hoa, S.V. and Liu, P. (2014), "A method to analyze the pure bending of tubes of cylindrically anisotropic layers with arbitrary angles including 0° or 90°",*Compos. Struct.*, **109**, 57-67.
Zozulya, V.V. and Zhang, C. (2012), "A high order theory for functionally graded axisymmetric cylindrical shells", *Int. J. Mech. Sci.*, **60**(1), 12-22.

CC

Appendix A

The linear global interpolation function is defined as (Yazdani Sarvestani 2011)

$$\phi_k(z)=\begin{cases}0 & z \le z_{k-1}\\ \psi_{k-1}^{2}(z) & z_{k-1}\le z \le z_k\\ \psi_k^{1}(z) & z_k \le z \le z_{k+1}\\ 0 & z \ge z_{k+1}\end{cases} \quad (k=1,2,...,N+1) \tag{A.1}$$

where $\psi_k^j(j=1,2)$ represent the local Lagrangian linear interpolation functions within the *k*th layer which are defined as

$$\psi_k^1(z)=\frac{1}{h_k}(z_{k+1}-z) \qquad \text{and} \qquad \psi_k^2(z)=\frac{1}{h_k}(z-z_k) \tag{A.2}$$

where h_k is the thickness of the *k*th layer.

Appendix B

The coefficient matrices [*M*], [*K*] and {*F*} in Eq. (17) are obtained as:

$$[M]=\begin{bmatrix}-[H_{66}] & -[H_{26}] & -\left([H_{26}]+[B_{36}]-[B_{45}]^T\right)\\ -[H_{26}] & -[H_{22}] & -\left([H_{22}]+[B_{23}]-[B_{44}]^T+[H_{44}]\right)\\ [0] & [0] & -[H_{44}]\end{bmatrix},$$

$$[K]=\begin{bmatrix}[A_{55}] & -[B_{45}]^T & [0]\\ [A_{45}]-[B_{45}] & [A_{44}]-[B_{44}]-[B_{44}]^T+[H_{44}] & [0]\\ -[B_{45}]+[H_{26}]+[B_{36}]^T & [H_{44}]-[B_{44}]+[H_{22}]+[B_{23}]^T & [H_{22}]+[B_{23}]+[B_{23}]^T+[A_{33}]\end{bmatrix}, \tag{B.1}$$

$$\{F\}=\begin{Bmatrix}\{0\} & -\{B_{16}\}\sin\theta & \{0\}\\ \{0\} & -\{B_{12}\}\sin\theta & \{0\}\\ \left(\{\bar{B}_{36}\}+\{B_{26}\}\right)\theta & -\left(\{\bar{B}_{13}\}+\{B_{12}\}\right)\sin\theta & -\left(\{A_{13}\}+\{F_{12}\}\right)\theta\end{Bmatrix}$$